



The catalytic performance of sulfated zirconia in the dehydration of methanol to dimethyl ether



Abd El-Aziz A. Said*, Mohamed M. Abd El-Wahab, Mohamed Abd El-Aal

Chemistry Department, Faculty of Science, Assiut University, 71516 Assiut, Egypt

ARTICLE INFO

Article history:

Received 23 May 2014

Received in revised form 28 June 2014

Accepted 30 June 2014

Available online 8 July 2014

Keywords:

ZrO₂

(NH₄)₂SO₄

Acidity

Methanol

Dimethyl ether

ABSTRACT

Sulfated zirconia catalysts were prepared by wetness impregnation of zirconium hydroxide with an aqueous solution of (NH₄)₂SO₄ with SO₄²⁻ loadings (1–30%, w/w) and calcined at 450 °C for 3 h in a static air atmosphere. The catalysts were characterized by FT-IR, XRD, TEM and BET measurements. The surface acidity of the catalysts was investigated by the dehydration of isopropanol and the adsorption of pyridine (PY) and 2,6-dimethyl pyridine (DMPY). The catalysts were tested for dehydration of methanol in a fixed-bed reactor at 230 °C using air as a carrier gas. The results revealed that among different catalysts, 10% SO₄²⁻ supported onto zirconia showed the highest catalytic activity with 83% conversion and 100% selectivity toward dimethyl ether. A good correlation was found between the acidity of the catalysts and their ability to dehydrate methanol.

© 2014 Elsevier B.V. All rights reserved.

1. Introduction

Dimethyl ether (DME) is a well-known building block in the production of valuable chemicals such as methyl acetate and dimethyl sulfate, as well as of petrochemicals (BTX aromatic and light olefins) and conventional fuels by replacing methanol as raw material. Moreover, DME is attracting increasing interest as a potential eco-friendly substitute for petroleum-derived diesel fuel given its high cetane number (55–60), low auto-ignition temperature, and reduced emissions of hazardous compounds such as NO_x, SO_x, and particulate matter [1,2]. DME may also serve as an efficient hydrogen carrier, which could be used to store renewable energy in a chemical form that is easy to handle, distribute, store and use [3]. DME can be produced by methanol dehydration over a solid-acid catalyst or direct synthesis from syngas by employing a hybrid catalyst, comprising a methanol synthesis component and a solid-acid catalyst [4]. The formation of DME from methanol requires a catalyst with optimum acid properties. Usually, strong acid sites favor secondary reactions that lead to undesired hydrocarbons and coke formation, which eventually causes catalyst deactivation [5]. A myriad of solid acid catalysts has been explored for the conversion of methanol into DME, including γ-Al₂O₃, modified alumina with silica, TiO₂–ZrO₂, and zeolite and zeotype materials (HZSM-5, HY, AlPO₄, SAPOs, etc.) [6]. Zeolite materials tend to deactivate rapidly

because their strong acid sites are responsible for the formation of significant amounts of undesired by-products (hydrocarbons and carbon deposits) [7]. On the other hand, γ-Al₂O₃, which possesses strong Lewis acid sites, exhibits lower methanol dehydration rates compared to zeolites, and thus, could be due to the preferential adsorption of generating H₂O molecules on the Lewis acid sites under the reaction conditions [5]. It is important to develop new catalysts to replace the acids commonly used in this reaction and to overcome the problems take place by using other solid acid catalysts. Sulfated zirconia is the most promising heterogeneous catalyst [8,9]. Its acidity is much higher even than that of concentrated H₂SO₄, with its surface sulfate groups acting as Lewis and Brønsted sites [10]. The high catalytic activity of sulfated zirconia has been attributed to super-acidity. In some cases, super-acids are significantly more active catalysts for reactions than conventional solid catalysts. Super Acid catalysts can offer many advantages: lower loadings, lower reaction temperatures, increased selectivity and fewer by-products, shorter reaction times. Satoshi et al. [11] studied the catalytic action of sulfated tin oxide for etherification and esterification of methanol in comparison with sulfated zirconia. Mohamed et al. [12] used methanol dehydration as a test reaction to compare the acidity of pure and sulfated metal oxides such as ZrO₂, TiO₂-anatase, -rutile and Al₂O₃. However, the catalytic dehydration of methyl alcohol to dimethyl ether on sulfated zirconia systems using air as a carrier gas, to our best knowledge, has not been reported. The objectives of the present study are prepared, characterization and evaluation of sulfated zirconia catalysts, for methanol dehydration to DME. Accordingly, the catalytic

* Corresponding author. Tel.: +20 882412427; fax: +20 882342708.

E-mail address: aasaid55@yahoo.com (A.E.-A.A. Said).

dehydration of methanol to DME was performed over a series of sulfated zirconia calcined at 450 °C for 3 h. Finally, an attempt has been made to correlate the catalytic activity of these catalysts, during dehydration of methanol, with their structure and the acidity.

2. Experiments

2.1. Materials

Zirconium hydroxide (Aldrich), ammonium sulfate $(\text{NH}_4)_2\text{SO}_4$, methyl alcohol, isopropyl alcohol, pyridine and 2,6-dimethyl pyridine were obtained as pure reagents and were used without further purification.

2.2. Catalyst preparation

A series of sulfated zirconia samples having different weight percentages of sulfate were synthesized by wetness impregnation of zirconium hydroxide with an aqueous solution of $(\text{NH}_4)_2\text{SO}_4$. Calculated amounts of ammonium sulfate were dissolved in small amounts of distilled water. The ammonium sulfate solutions were admixed carefully with calculated amounts of zirconium hydroxide till the formation of homogeneous pastes. The samples were dried in an oven at 100 °C for 24 h. The contents of SO_4^{2-} were (1, 3, 5, 10, 20 and 30 wt.%) before being calcined at 450 °C for 3 h in static air atmosphere. Sulfated zirconia catalyst donated by (SZ).

2.3. Catalyst characterization

2.3.1. Fourier transform infrared (FT-IR) spectroscopy

FT-IR spectra of the prepared catalysts calcined at 450 °C for 3 h were recorded using a Shimadzu Spectrophotometer, model (Nicolet 6700), equipped with data station in the range of 4000–400 cm^{-1} with a KBr disc technique.

2.3.2. X-ray diffraction (XRD)

XRD analysis of the test samples was performed with a Philips (The Netherlands) diffractometer (Model PW 2103, $\lambda = 1.5418 \text{\AA}$, 35 kV and 20 mA) with a source of $\text{CuK}\alpha$ radiation (Ni filtered). Patterns were recorded from 4 to 80° (2θ). Particle size was estimated using Scherrer equation [13]:

$$D = \frac{K\lambda}{\beta \cos \theta}$$

where D is the mean crystallite diameter (nm), λ is the X-ray wavelength, K is Scherer constant (0.89), β is the observed angular width at half maximum intensity of the peak and was calculated by the following equation [14]:

$$\beta^2 = \beta_s^2 - \beta_o^2$$

where β_s is the full width of a diffraction peak under consideration (radian) in the middle of its height that was considered after computer fit of X-ray data using the Gaussian line shape and θ is the Bragg's angle and β_o is the instrumental broadening, $\beta_o = 0.16$ with the apparatus used.

2.3.3. Transmission electron microscopy (TEM)

The size and morphology of the investigated catalysts were characterized by transmittance electron microscope (TEM) JEOL Model JSM-5400 LV (Joel, Tokyo, Japan). The catalyst powder dispersed in ethanol using ultrasonic radiation for 20 min and a drop of that suspension was placed onto the carbon-coated grids. The degree of magnification of TEM images was the same for all the different investigated catalysts.

2.3.4. Nitrogen gas adsorption

Nitrogen gas adsorption–desorption isotherms were measured at –196 °C using a Nova 3200 instrument (Quantachrom Instrument Corporation, USA). Test samples were thoroughly outgassed for 3 h at 250 °C to a residual pressure of 10^{-5} Torr, and the weight of the outgassed sample was that used in calculations. The specific surface area, S_{BET} was calculated by applying the Brunauer–Emmett–Teller (BET) equation. The porosity of the catalysts was determined from the desorption curves using Nova enhanced data reduction software (Version 2.13). The theoretical particle sizes are also calculated from specific surface area, assuming spherical particles according to the following equation:

$$D_{\text{BET}} = \frac{6000}{p \cdot S_{\text{BET}}}$$

where D_{BET} is the average particle size (nm), p is the theoretical density of the sample (g cm^{-3}) and S_{BET} is the specific surface area ($\text{m}^2 \text{ g}^{-1}$).

2.3.5. Acidity determination

The acidity of the catalysts under investigation were determined by studying the dehydration of isopropyl alcohol (IPA), the adsorption of pyridine (PY) and 2,6-dimethyl pyridine (DMPY). The dehydration of IPA was carried out in a conventional fixed-bed flow Pyrex glass tube reactor, at atmospheric pressure using nitrogen as a carrier gas. The reaction conditions were: A 500 mg catalyst, 2% reactant of IPA in the gas feed, 50 ml min^{-1} total flow rate and 200 °C reaction temperature. The measurement of propene yield (%) was made after 1 h to achieve steady-state reaction conditions of the IPA. The chemisorptions of PY and DMPY were carried out by injection of different volumes at steady state conditions. The exit feed was analyzed by direct sampling of the gaseous products into a Unicam ProGC gas chromatograph using a flame ionization detector (FID) with a 10% PEG 400 glass column (2 m). The acidity populations over the surface of catalysts, under investigation, were measured also by thermogravimetric technique (TG) using the adsorption of pyridine as probe molecule. The procedure was 500 mg of calcined sample was preheated at 250 °C for 1 h in the air before saturated with pyridine for 7 days after evacuation. About 15 mg of pyridine-saturated sample was subjected to TG analysis. The TG analysis was recorded heating from room temperature up to 400 °C using at 10 °C min^{-1} and 30 ml min^{-1} flow of N_2 , using Computerized Shimadzu Thermal Analyzer TA60 Apparatus (Japan). The mass loss due to desorption of pyridine from the acidic sites, was determined as a function of total surface acidity as sites ($\text{g}^{-1}_{\text{cat}}$) [15].

2.3.6. Catalytic activity measurements

The catalytic activity of the catalysts under investigation for the vapor – phase dehydration of methyl alcohol was carried out at 230 °C in a conventional fixed bed flow type reactor at atmospheric pressure using air as the carrier gas. The system comprised two reactors. One was used without any catalyst and filled with glass beads (control reactor), to enable a measurement of the 'control' conversion (if any), which was subtracted from that measured in the flow reactor. 500 mg of catalyst was placed in the middle of the second reactor with quartz wool. Space in the reactor pre- and post-heating zone was filled with glass beads to reduce the effect of auto-oxidation of the substrate and products in the gas phase. A methyl alcohol and air were introduced into the reactor after air was bubbled through methyl alcohol saturator. The total flow rate was fixed at 50 ml min^{-1} and used 4% reactant of methanol in the gas feed. The gases after reaction were chromatographically analyzed by FID with a Unicam ProGC using a 2 m DNP glass column for analysis of the reaction products of methyl alcohol on the tested catalysts. Measurements

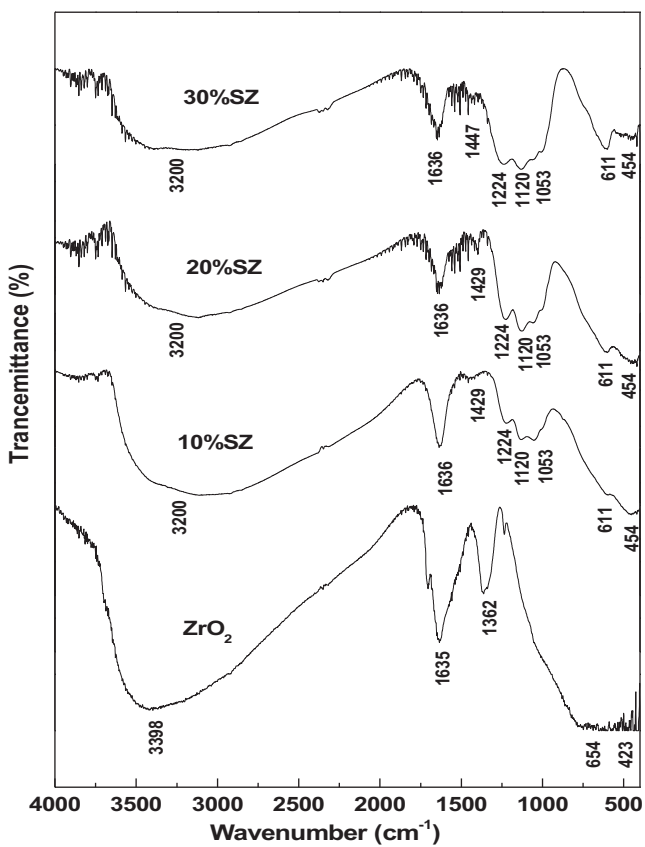


Fig. 1. FTIR spectra of non-sulfated and sulfated zirconia calcined at 450 °C for 3 h.

of the conversion and yield (%) were recorded after 1 h from the initial introduction of the reactant into the reactor to ensure the attainment of the reaction equilibrium, (steady state conditions).

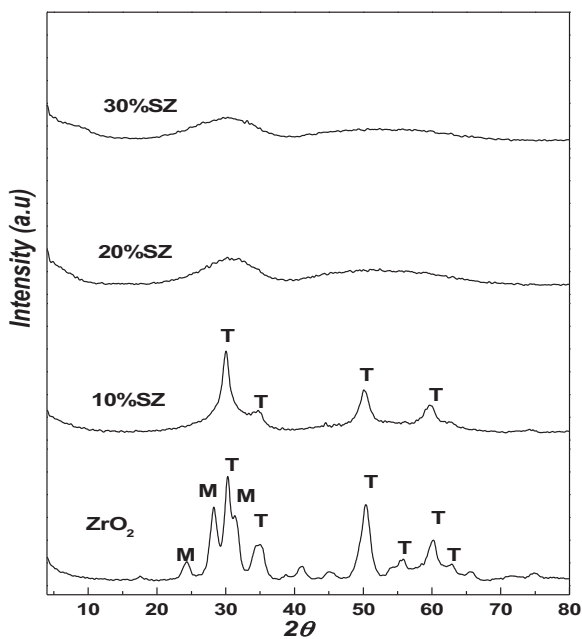
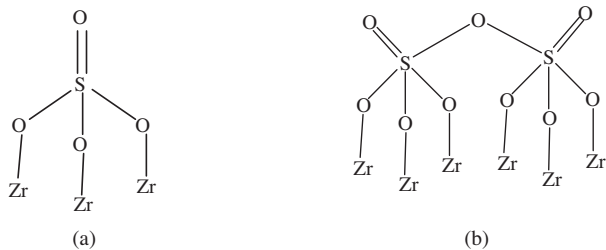


Fig. 2. X-ray diffractograms of non-sulfated and sulfated zirconia calcined at 450 °C for 3 h.

3. Results and discussion

3.1. Infrared analysis of zirconia and sulfated zirconia

FT-IR spectra of pure ZrO₂ and sulfated with 10, 20 and 30 wt.% calcined at 450 °C were measured in the range 4000–400 cm⁻¹ and presented in Fig. 1. It shows that, the FT-IR spectrum for pure ZrO₂, the bands assigned at 423–654 cm⁻¹ are corresponded to Zr—O—Zr bond [16]. A strong and broad band with a maximum centered at 3398 cm⁻¹ which is attributed to physisorbed water, whereas the band at 1635 cm⁻¹, assigned to the bending mode (ν_{HOH}) of coordinated water [17]. The band at 1362 cm⁻¹ was assigned to the bending vibration of Zr—OH groups [18]. The FT-IR spectra of sulfated zirconia catalysts show bands at 1053, 1120 and 1224 cm⁻¹. These bands are assigned to asymmetric and symmetric stretching modes of oxygen bound to the sulfur of sulfate [19]. Moreover, the band assigned at 1429 cm⁻¹ is due to the presence of S=O stretching vibration of the surface sulfate species [20]. The wave number of this band increases with the sulfur content, due to a change in the type of sulfate species from isolated ones (a) to poly nuclear ones (b) [21].



The partially ionic nature of the S=O bond is responsible for the Brønsted acid sites in sulfated zirconia samples [22]. Furthermore, the band observed at 1636 cm⁻¹ is due to the bending vibration mode of an O—H group of water associated with the sulfate. The broad band around 3200 cm⁻¹ is attributed to the O—H stretching vibration of water associated with ZrO₂ and the broadness indicates the effect of hydrogen bonding [20]. It is worth mentioning here that the O—H stretching, vibration band decreases by the increasing percentage loading of SO₄²⁻. This behavior may be attributed to the successive formation of H₂SO₄, HSO₄⁻ and SO₄²⁻ from water sensitive SO₃ groups [23].

3.2. X-ray diffraction (XRD)

The XRD patterns of sulfated and non-sulfated zirconia samples calcined at 450 °C are presented in Fig. 2. The pure ZrO₂ sample exhibits both tetragonal ($2\theta = 30.3^\circ, 35.3^\circ, 50.7^\circ, 59.9^\circ, 60.6^\circ$ and 63.5° [24]) and monoclinic ($2\theta = 24.7^\circ, 28.4^\circ, 31.6^\circ$ [25]) phases, whereas only tetragonal phase is observed in the sulfated sample containing 10 wt.%. This behavior suggests that the presence of sulfate within dried Zr(OH)₄ before calcination is responsible for inhibiting the crystal phase transformation from tetragonal to monoclinic. The change in the crystal phase is due to the strong interaction between the OH groups of ZrO₂ and the sulfate ions of (NH₄)₂SO₄ to form a chemically stable SO₄/ZrO₂ complex [26]. These results are in good agreement with the results reported by Mishra et al. [27]. On the other hand, the disappearance of the characteristic peaks of tetragonal and monoclinic (amorphous) phases of the samples with loading above 10% (w/w) reflects the high dispersion of SO₄²⁻ in the porous zirconia. However, the diffraction peak at 2θ values of 30.1° was selected for calculating the crystallite size of samples calcined at 450 °C. The crystallite sizes of samples calcined at 450 °C are cited in Table 1. The results obtained demonstrate that crystalline sizes, decreases with the addition of sulfate with 10 wt.%. These results are confirmed by the results

Table 1

Texture data of sulfated and non-sulfated zirconia calcined at 450 °C for 3 h.

SO_4^{2-} (%)	S_{BET} ($\text{m}^2 \text{ g}^{-1}$)	Total pore volume (ccg^{-1})	Average pore diameter (\AA)	D_{XRD} (nm) ^a	D_{BET} (nm) ^b
Pure ZrO_2	120.6	0.1674	55.5	9.5	8.76
1%	158.2	0.1476	35.8	–	6.67
3%	184.9	0.1397	30.2	–	5.71
5%	185.8	0.1290	27.8	–	5.68
10%	178.3	0.1152	25.8	4.9	5.90
20%	107.3	0.0688	25.7	–	22.6
30%	46.70	0.0574	49.2	–	51.8

^a Crystalline size: determined by XRD results.

^b Particle size: determined by BET surface area.

reported by Mishra et al. [27]. A further increase in the amount of SO_4^{2-} (more than 10 wt.%) resulted in the formation of amorphous samples which is difficult to calculate the crystalline sizes of these samples from their XRD patterns.

3.3. Transmission electron microscope (TEM)

To precise the morphology and size of the nanoparticles determination, TEM is more suitable and powerful tool. Fig. 3 shows the TEM micrographs of pure ZrO_2 and 10% SZ calcined at 450 °C for 3 h. It can be observed that the presence of agglomerates of semi-spherical nanosized particles and the powders are uniform in size. It can also notice that the particle sizes of a 10% SZ are smaller than that of pure ZrO_2 . The mean particle size of both samples observed from TEM image is larger than the crystalline size estimated from XRD and surface area analysis, which could be attributed to the crystalline agglomeration through heat treatment [28].

3.4. Surface area measurements

All isotherms (not shown) for pure zirconia and different loadings of SZ calcined at 450 °C were found to be of type IV, which are generally observed for mesoporous solids. However, there is a large increase in adsorption at a higher relative pressure showing the presence of larger size mesopores in the samples. The inflection point for pure zirconia at around $p/p^0 = 0.4$, is not sharp, which reflects that the pores are not uniform in size and have broad distribution. The hysteresis loop belongs to type H2 of de Boer classification [29] for pure zirconia, 1, 3, 5, 10 and 20% SZ, while for 30% SZ the hysteresis loop belongs to H3 type. In addition, the hysteresis loop of pure zirconia with a wider gap, while on increasing the addition of % SO_4^{2-} the gap becomes narrower. The BET

surface areas, theoretical particle sizes, pore volume and average pore diameter of sulfated and non-sulfated zirconia samples are presented in Table 1. It shows that, pure ZrO_2 exhibits a surface area of $120.6 \text{ m}^2 \text{ g}^{-1}$. In addition of (1–5) wt.% SO_4^{2-} , the surface area significantly increases to $185.8 \text{ m}^2 \text{ g}^{-1}$ and thereafter decreased. All the samples are essentially mesoporous materials (Average pore diameter between 25 and 55.5 Å). The pore volume is between 0.0574 and 0.1674 cc g^{-1} . The theoretical particle sizes of pure ZrO_2 and 10% SZ samples that calculated from surface area are close to the crystalline sizes that calculated from XRD analysis. So, it is clear from the texture investigation of prepared catalysts that, sulfating of ZrO_2 causes an enormous increase of the surface area with concomitant decrease of pore diameter, pore volume and particle size with loadings up to 10%.

3.5. Determination of the surface acidic sites

3.5.1. Dehydration of isopropyl alcohol

The catalytic dehydration of isopropyl alcohol (IPA) over pure ZrO_2 and sulfated zirconia calcined at 450 °C are carried out and the results are shown in Fig. 4. The results indicate that the reaction product of IPA was only propene. However, the dehydration reaction of IPA catalyzed at acidic sites has been used by several authors [30,31] as a test reaction for determining the acidity. Thus, it can be observed from Fig. 5 that ZrO_2 is an inactive catalyst toward IPA reaction under our conditions. Eventually, the addition of SO_4^{2-} sharply increases the dehydration capacity, reaching a maximum at 10 wt.%, then gradually decreases up to 30 wt.%. The difference between the performances of the supported catalysts is explained on the basis of SO_4^{2-} interaction with the ZrO_2 support via creation of more acidic sites, which is responsible for the dehydration reaction.

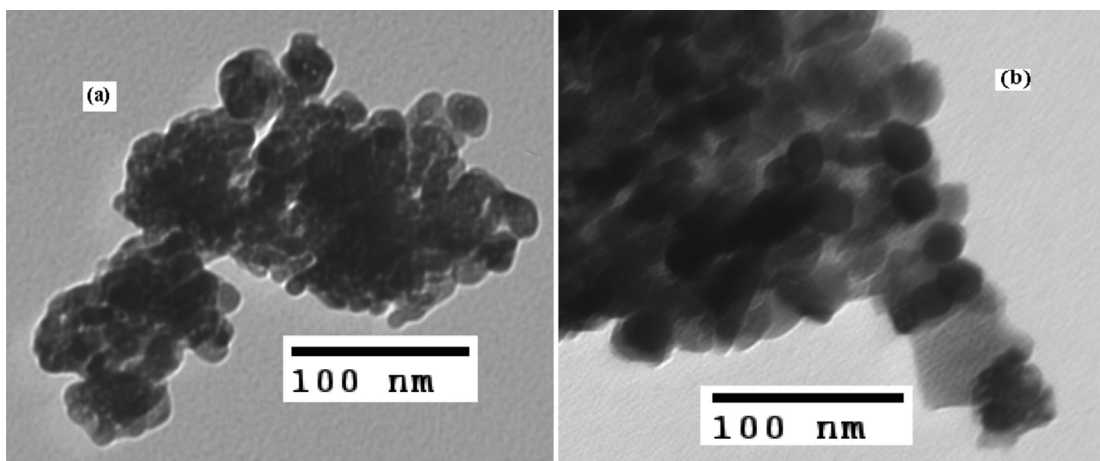


Fig. 3. TEM images of (a) pure ZrO_2 and (b) 10% SZ calcined at 450 °C for 3 h.

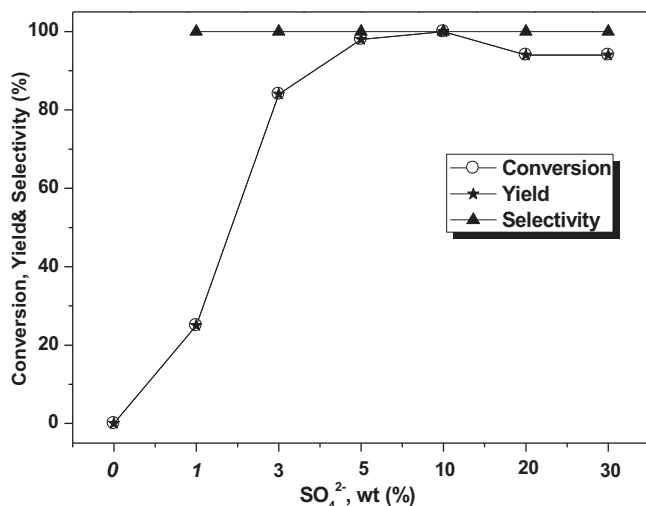


Fig. 4. Activity variation of IPA with % SO_4^{2-} loading on ZrO_2 calcined at 450 °C for 3 h.

3.5.2. Poisoning of acid sites with pyridine and 2,6-dimethyl pyridine over 10% (SZ) catalyst during the reaction of IPA

It is known that the chemisorption of pyridine (PY) and 2,6-dimethyl pyridine (DMPY) can be used as basic probe molecules to determine the acidity of a catalyst [32]. It was reported that PY is selectively adsorbed on both Brønsted (B) and Lewis (L) acid sites [33]. On the other hand, DMPY is selectively adsorbed on (B) acid site [34] but not (L) sites because of the steric hindrance of two methyl groups. So the difference between PY and DMPY adsorption is a measure of the (L) acid sites. The poisoning of the active surface sites of 10% SZ catalyst in IPA conversion was performed through saturation of the acid sites with PY or DMPY according to the following procedures. After measuring the conversion activity of the 10% SZ catalyst toward the dehydration of IPA at 200 °C the catalyst

was injected with different volumes of PY or DMPY in the stream of the reactants using N_2 as a carrier gas. Fig. 5 represents the effect of PY and DMPY additions on the distribution products of the IPA reaction on 10% SZ catalyst. The results show that the injection of PY or DMPY led to a continuous decrease in the conversion of IPA and the yield of propene up to the addition of 6 μL then a steady state is reached. This means that PY and DMPY suppressed IPA dehydration activity. Thus, the chemisorbed PY and DMPY decrease the yield of the propene by ≈97 and 92%, respectively on the addition of 6 μL . It is clear from the above results that there is a little difference (≈5%) between the amount adsorbed from PY and DMPY, which is corresponding to the presence of (L) acid sites. Thus, the catalyst with 10% SZ is an acidic catalyst with major (B) acid sites and minor (L) acid sites. This finding is in good agreement with the results that obtained by Kemnitz et al. [35]. In addition the existence of a high concentration of (B) relative to (L) acid sites was expected as a result of moisture adsorption; Zhang et al. [36].

3.5.3. Thermal analysis of 10% SZ presaturated with pyridine

DSC, TG and DTA curves of the desorption of PY from presaturated 10% SZ catalyst are carried out and presented in Fig. 6. The TG curve exhibits a total weight loss of about 12.3% through two steps. The first step lies in the temperature range of (29–100 °C). This step is associated with a strong endothermic peak on the DTA curve minimized at 62 °C. This peak may be attributed to the removal of adsorbed water and desorption of PY molecules from weak acid sites. The second step lies in the temperature range of (100–250 °C) and is not accompanied by any peak in the DTA curve. This behavior may indicate that the removal of PY of weak and intermediate acid sites occurs without gain or release energy. The DSC curve shows only one endothermic peak minimized at 105 °C. This peak covered the temperature range from 50 to 200 °C and may be attributed to the removal of PY of weak and intermediate acid sites. So, it is clear from the above results that, the catalyst containing 10% SO_4^{2-} exhibits an acidic catalyst with weak and intermediate (major) acidic sites.

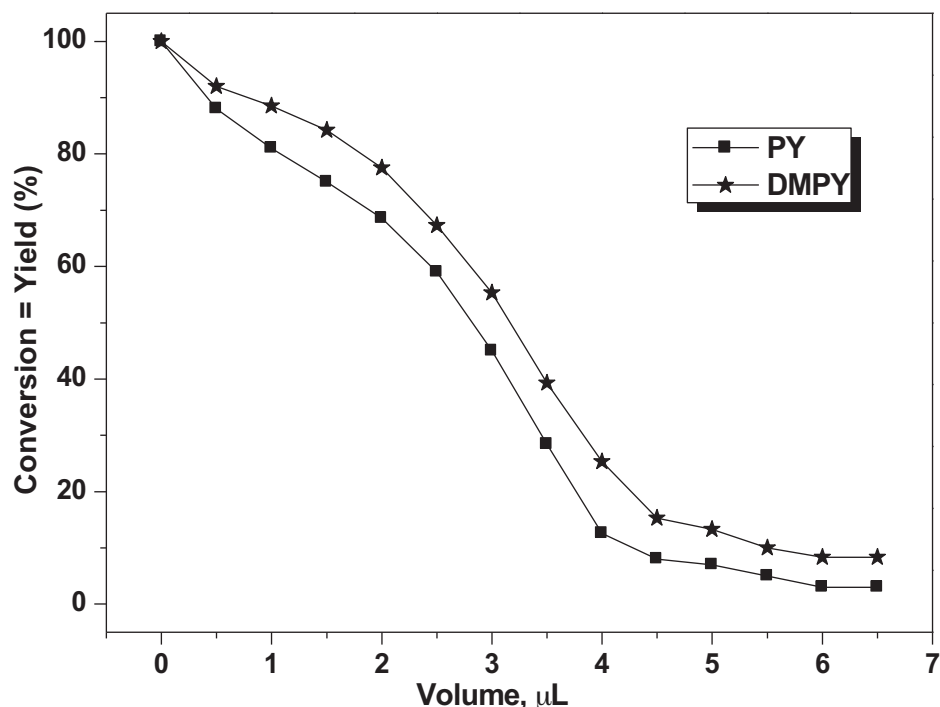


Fig. 5. Activity variation of IPA with the volume of PY and DMPY over 10% SZ catalyst calcined at 450 °C for 3 h.

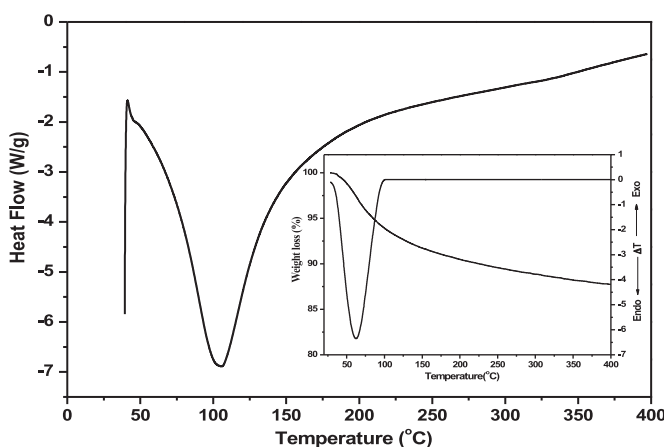


Fig. 6. DSC, TG and DTA curves of desorption of PY from 10% SZ catalyst.

3.5.4. Effect of reaction temperature on the dehydration of IPA over 10% SZ catalyst presaturated with PY and DMPY

It was reported that [37] the activity of solid – acid catalysts depends on many factors, but the (B) acid site density is usually one of the most crucial parameters. However, it is known that (B) and (L) acid sites are capable of retaining pyridine at certain temperatures. The poisoning of the active acidic sites of 10% SZ catalyst under investigation was performed through the previous saturation of the acidic sites with PY and DMPY for 7 days after evacuation. The unsaturated and saturated catalyst was subjected to the catalytic reaction of IPA under different reaction temperatures using similar conditions of the catalytic runs as mentioned above and the results are shown in Fig. 7. It shows that the saturation of catalyst with PY or DMPY retards its catalytic activity to higher temperature. This retardation means that PY and DMPY molecules prevent the (B) acid sites to react with IPA. According to DSC, TG and DTA results (Fig. 6), it can be observed that the chemisorbed molecules of PY and DMPY need energy to be removed from weak and medium strength (B) acid sites in the range of temperature of (50–200 °C). So, the results presents in Fig. 7 go parallel with that shown in Fig. 6. On increasing the reaction temperature, the catalyst restores its original catalytic activity at 275 °C. The obtained results indicate that there is a little difference between the conversion of the IPA and the yield of propene over the catalyst saturated with PY or DMPY. This behavior reflects that the catalyst exhibits acidity with almost (B) type. This is in good agreement with the results that obtained in case of chemisorption of PY and DMPY during the catalytic dehydration of

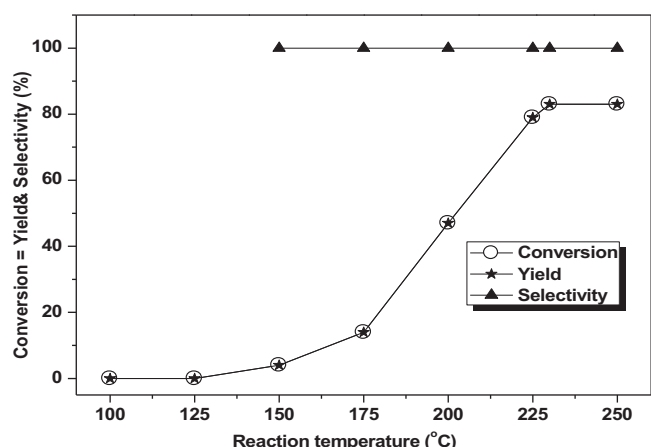


Fig. 8. Effect of reaction temperature on the dehydration of methanol over 10% SZ catalyst calcined at 450 °C using air or nitrogen as a carrier gas.

IPA see Fig. 5. In conclusion, the results of the acidity determination formulate that the investigated catalysts have mainly acidic sites of (B) type, with weak and medium strengths.

3.6. Catalytic activity

It is well known that methanol conversion can carry on a solid-acid catalyst either as simply dehydration producing only DME and water or as deep dehydration, yielding hydrocarbons [7]. Previous researchers have reported that the (B) acid or (L) acid sites are the active sites for methanol dehydration to DME [38]. It is commonly agreed that (B) acid sites of medium strength are required to obtain high reaction rates without causing relevant deactivation phenomena [5,39]. The effect of reaction temperature on the catalytic dehydration of methanol in the range 100–275 °C over 10% SZ catalyst calcined at 450 °C was carried out under air and nitrogen. The percentages of conversion, yield and selectivity were represented in Fig. 8. It shows that the reaction started at 150 °C and the methanol conversion and yield of DME increase monotonically with increasing the reaction temperature up to 230 °C. With increasing the reaction temperature up to 250 °C constant values of methanol conversion and yield of DME were obtained by using air or nitrogen as a carrier gas. By raising the reaction temperature up to 275 °C and using air as a carrier gas, the yield of DME drastically decreased and methanol oxidized to CO₂ and CO products. No oxidation of methanol is observed at 275 °C with constant values of conversion and yield of DME when using nitrogen as a carrier gas. The above results indicate that the optimum reaction temperature is 230 °C under both air and nitrogen is accompanied with 83% yield and 100% selectivity to DME. However, G. Lauget et al. [40], studied methanol dehydration into dimethyl ether over ZSM-5 type zeolites under inert and oxidative atmosphere. They found that using air as a carrier gas inhibit the methanol-To-Hydrocarbons (MTH) reaction and also prevent the deactivation of MFI zeolite and increase its stability at 275 °C.

The effect of catalyst calcination temperature on the catalytic activity of a 10% SZ toward methanol dehydration was studied on the catalyst calcined at 300, 350, 400, 450 and 500 °C using air as a carrier gas and the results are cited in Table 2. The experimental results revealed that a significant increase in methanol conversion as well as DME yield is observed up to calcined at 450 °C. With increasing the calcination temperature to 500 °C the catalyst lost a certain amount of its water. It was proposed earlier [41] that for a catalyst to be effective in methanol dehydration, a minimum amount of water is necessary. In addition, the same substance within a certain concentration of water limits acted as

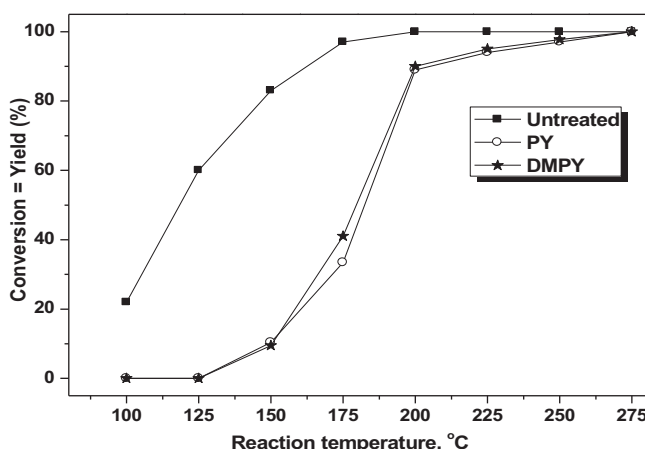


Fig. 7. Activity variation of IPA with reaction temperature over 10% SZ catalyst and saturated with PY and DMPY.

Table 2

Effect of catalyst calcination temperature on the dehydration of methanol over 10% SZ catalyst using air as a carrier gas.

Calcination temperature (°C)	Conversion (%)	Selectivity (%)	Yield of DME (%)
300	69	100	69
350	74	100	74
400	80	100	80
450	83	100	83
500	76	100	76

a catalytic promoter. On the other hand, a higher concentration of water may be poisoned the catalyst. So, the effect of calcination temperature on the catalysts suggests that the water present in these catalysts played an important role in their activities in methanol dehydration. Ki-Won Jun et al. [42] stated that the dehydroxylated $\text{SiO}_2\text{-Al}_2\text{O}_3$ becomes rather hydrophobic resulting in the decrease of sorption capacity of water. They also mentioned that water blocks the active sites for methanol dehydration through competitive adsorption with methanol on the catalyst surface. This is why the catalyst calcined at lower temperature showed lower activity. Besides, the high calcination temperature may change the strength of the acidity. Consequently, we can suggest that the optimum value of water needed to make the catalyst under investigation exhibits higher activity and selectivity should be calcined at 450 °C.

The effect of sulfate loadings on dehydration of methanol over the catalysts calcined at 450 °C in presence air as a carrier gas is shown in Fig. 9. The results reveal that pure zirconia has no activity toward methanol dehydration under our conditions. This behavior may be explained on the basis of the catalyst has no acidity as observed in the acidity determination see Fig. 4. On the other hand, sulfated zirconia shows a significant increase in both conversion and yield toward the formation of DME on increasing the SO_4^{2-} reaching a maximum at the addition of 10 wt.%, then gradually decrease up to the addition of 30 wt.%. The maximum yield of DME ($\approx 83\%$) is obtained over 10% SZ with selectivity of 100%. As mentioned earlier [43], sulfating of zirconia induces the structural stabilization of the tetragonal phase as seen from X-ray results in Fig. 2, which is known to associate with the catalyst activity. Srinivasan et al. [44] suggested that oxygen adsorption by oxygen deficient surface sites could be responsible for the transition of the tetragonal phase into monoclinic phase at low temperatures. They also showed that the presence of sulfate ions would protect the surface against oxygen adsorption and so the transition of the tetragonal phase into monoclinic phase would be prevented.

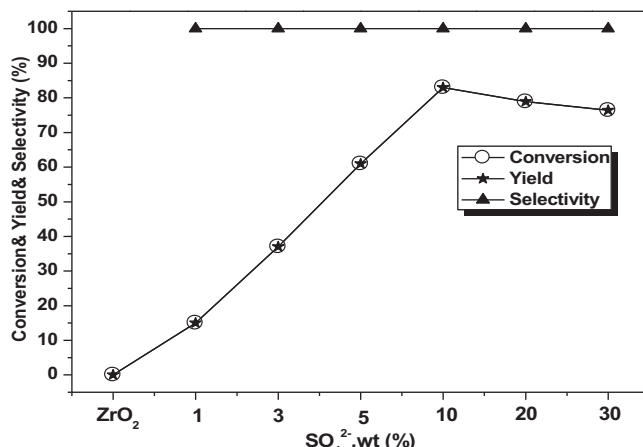


Fig. 9. Effect of sulfate loadings on dehydration of methanol over catalysts calcined at 450 °C for 3 h using air as a carrier gas.

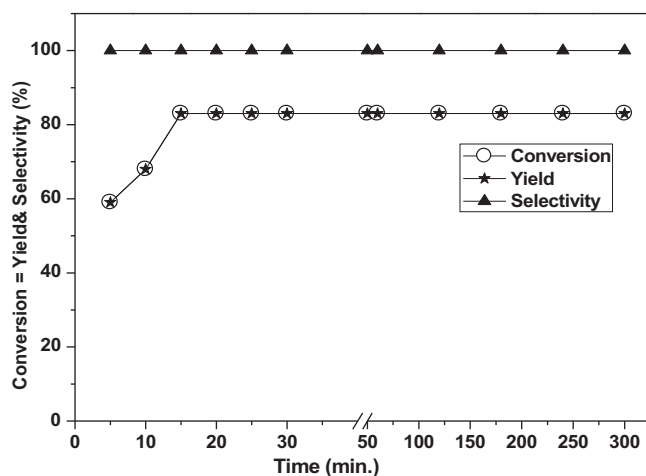


Fig. 10. Effect of reaction time on the catalytic dehydration of methanol over 10% SZ catalyst calcined at 450 °C.

Moreover, such a process enhances the catalyst acidity amount and retards the particle aggregation, which leading to smaller particle size and larger surface area as seen in Table 1.

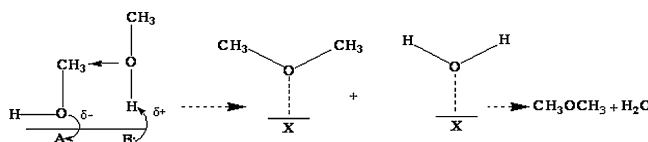
3.7. Stability of 10% SZ catalyst

To evaluate the stability of the 10% SZ catalyst, the dehydration of methanol to DME was investigated using air as a carrier gas and the results are presented in Fig. 10. It shows that the maximum conversion of methanol (83%) with 100% selectivity to DME was observed after 15 min from the introduction of the reactant followed by steady till 300 min. However, for the application of $\text{SO}_4^{2-}/\text{M}_x\text{O}_y$ in various reactions, deactivation is the fatal problem [45]. Nowadays, the main mechanism of solid super acid deactivation can be described as follows: first, the lost of SO_4^{2-} [46] as a result of the presence of water or vapor in contact with SO_4^{2-} during catalytic reactions, which caused the acid sites number to decrease and weakened the acid strength, leading the catalyst's activity to decline and second, carbon coke [47]. To regenerate the used catalyst, Li and Gonzalez [48] have determined that calcining a deactivated conventional sulphated zirconia catalyst in oxygen at 450 °C is critical in regaining the original activity. It is of interest to mention here that under our reaction conditions the sulphated zirconia catalysts not undergo any deactivation. This behavior due to the use of air as a carrier gas which prevent the deactivation of the catalyst. It was reported that the presence of air allows to maintain the catalyst surface active, via reducing the deactivation probably by burning hydrocarbons present in the zeolite micropores [40].

3.8. Mechanism of methanol dehydration

During the dehydration of alcohol, both intramolecular and intermolecular dehydration may occur. The relative amounts of these pathways depend on the reaction conditions as well as the reactant and catalyst used. The first step of alcohol conversion on metal oxide catalysts is the adsorption of the reactant on the surface. The adsorbed alcohols can be converted through a two-step mechanism involving the intermediate carbocation formation (E1), a concerted pathway (E2) or via carbanion formation mechanism (E1cb) [49]. E1 mechanism needs a strong acidic catalyst to form carbium ions by abstraction of OH group. The carbium ion is rearranged via isomerization followed by abstraction of a β -hydrogen resulting in the thermodynamically controlled alkenes. For E2 mechanism, reaction occurs at dual acid-base sites to eliminate a proton and a hydroxyl group. Whereas for E1cb mechanism,

strong basic sites are required in order to initially remove a β -hydrogen and then eliminate the hydroxyl group. The presence of an asymmetric vibrational mode of S=O is considered to be associated with the promotion of more surface acidity over SZ catalysts [50]. It is known that the acid strength of $Zr^{\delta+}$ becomes stronger due to the inductive effect of S=O in the SO_4/ZrO_2 complex. Sulfated zirconia surface contained Brønsted acidic and basic hydroxyl groups, so we suggested that sulfated zirconia catalysts dehydrate methanol via E2 mechanism. Two molecules of CH_3OH adsorbed on a surface oxide, one is adsorbed on the acid site (B site) and another molecules adsorbed on the basic site (hydroxyl group) and forming an intermediate which decomposes to give DME and water. Accordingly, the dehydration of methanol can be proceeded as follows:



4. Conclusion

Dimethyl ether can be conveniently synthesized by vapor phase dehydration of methanol using various oxides, mixed oxides and their sulfated forms as the catalysts. Sulfated zirconia proves to be a good catalyst for this reaction. Thus, the 10% SZ catalyst under our optimum conditions has been found to be an efficient catalyst for the synthesis of dimethyl ether with high yield (83%) and excellent selectivity (100%). Moreover, using of air as a carrier gas prevented the deactivation of the prepared catalysts toward DME formation. This finding is a value added to the advantages of using sulfated zirconia in dehydration of methanol to dimethyl ether.

References

- [1] T.A. Semelsberger, R.L. Borup, H.L. Greene, J. Power Sources 156 (2006) 497–511.
- [2] C. Arcoumanis, C. Bae, R. Crookes, E. Kinoshita, Fuel 87 (2008) 1014–1030.
- [3] S.S. Akarmazyan, P. Panagiotopoulou, A. Kambolis, C. Papadopoulou, D.I. Kon-darides, Appl. Catal. B: Environ. 145 (2014) 136–148.
- [4] A.R. Keshavarz, M. Rezaei, F. Yaripour, J. Nat. Gas Chem. 20 (2011) 334–338.
- [5] R. Ladera, E. Finocchio, S. Rojas, G. Busca, J.L.G. Fierro, M. Ojeda, Fuel 113 (2013) 1–9.
- [6] R. Ladera, E. Finocchio, S. Rojas, J.L.G. Fierro, M. Ojeda, Catal. Today 192 (2012) 136–143.
- [7] G.R. Moradi, F. Yaripour, P. Vale-Sheyda, Fuel Process. Technol. 91 (2010) 461–468.
- [8] Y. Wu, S. Liao, Front. Chem. Eng. Chin. 3 (2009) 330–343.
- [9] V.K. Ivanov, A.Ye. Baranchikov, G.P. Kopitsa, S.A. Lermontov, L.L. Yurkova, N.N. Gubanova, O.S. Ivanova, A.S. Lermontov, M.N. Rumyantseva, L.P. Vasilyeva, M. Sharp, P.K. Pranzas, Y.D. Tretyakov, J. Solid State Chem. 198 (2013) 496–505.
- [10] J.R. Sohn, J. Ind. Eng. Chem. 10 (2004) 1–15.
- [11] S. Furuta, H. Matsuhashi, K. Arata, Appl. Catal. A: Gen. 269 (2004) 187–191.
- [12] M. Waqif, J. Bachelier, O. Saur, J.C. Lavalle, J. Mol. Catal. 72 (1992) 127–138.
- [13] B.D. Cullity, Elements of X-ray Diffraction, 3rd ed., Addison-Wesley, Reading, MA, 1967.
- [14] B.A. Reguig, A. Khelil, L. Cattin, M. Morsli, J.C. Bernède, Appl. Surf. Sci. 253 (2007) 4330–4334.
- [15] A.I. Osman, J.K. Abu-Dahrieh, D.W. Rooney, S.A. Halawy, M.A. Mohamed, A. Abdolkader, Appl. Catal. B: Environ. 127 (2012) 307–315.
- [16] F. Heshmatpour, R.B. Aghakhanpour, Adv. Powder Technol. 23 (2012) 80–87.
- [17] A. Sinhamahapatra, N. Sutradhar, M. Ghosh, H.C. Bajaj, A.B. Panda, Appl. Catal. A: Gen. 402 (2011) 87–93.
- [18] X. Dou, D. Mohan, C.U. Pittman Jr., S. Yang, Chem. Eng. J. 198–199 (2012) 236.
- [19] D. Radwan, L. Saad, S. Mikhail, S.A. Selim, J. Appl. Sci. Res. 5 (12) (2009) 2332–2342.
- [20] V. Vishwanathan, G. Balakrishna, B. Rajesh, V. Jayasri, L.M. Sikhwivhilu, N.J. Coville, Catal. Commun. 9 (2008) 2422–2427.
- [21] M.T. Tran, N.S. Gnepp, G. Szabo, M. Guisnet, Appl. Catal. A: Gen. 171 (1998) 207–217.
- [22] M.K. Mishra, B. Tyagi, R.V. Jasra, J. Mol. Catal. A: Chem. 223 (2004) 61–65.
- [23] V.G. Deshmame, Y.G. Adewuyi, Appl. Catal. A: Gen. 462–463 (2013) 196–206.
- [24] E.A. Garcia, E.H. Rueda, A.J. Rouco, Appl. Catal. A: Gen. 210 (2001) 363–370.
- [25] T. Yamamoto, T. Tanaka, S. Takenaka, S. Yoshida, T. Onari, Y. Takahashi, T. Kosaka, S. Hasegawa, J. Phys. Chem. B 103 (1999) 2385–2393.
- [26] S. Narayanan, M.S. Krishnan, V. Vishwanathan, J. Mater. Sci. 30 (1995) 6355–6358.
- [27] H.K. Mishra, K.M. Parida, Appl. Catal. A: Gen. 224 (2002) 179–189.
- [28] S. Bai, D. Li, D. Han, R. Luo, A. Chen, C.C. Liu, Sensors Actuat. B: Chem. 150 (2010) 749–755.
- [29] J.H. De Boer, E.P. Everette, F.S. Stone (Eds.), The Structure and Properties of Porous Materials, Butterworths, London, 1958, p. 68.
- [30] J.R. Sohn, H.J. Jang, J. Mol. Catal. 64 (1991) 349–360.
- [31] A.A. Said, J. Chem. Technol. Biotechnol. 78 (2003) 733–742.
- [32] A.A. Said, M.M.M. Abd El-Wahab, A.M. Alian, J. Chem. Technol. Biotechnol. 82 (2007) 513–523.
- [33] M. Ziolek, J. Kujawa, O. Saur, A. Aboulayt, J.C. Lavalle, J. Mol. Catal. A 112 (1996) 125–132.
- [34] F.M. Bautista, J.M. Campelo, A. Garcia, D. Luna, J.M. Marinas, M.C. Moreno, A.A. Romero, Appl. Catal. A 170 (1998) 159–168.
- [35] V. Quaschning, J. Deutsch, P. Druska, H.J. Niclas, E. Kemnitz, J. Catal. 177 (1998) 164–174.
- [36] C. Zhang, R. Miranda, B.H. Davis, Catal. Lett. 29 (1994) 349–359.
- [37] O. Kresnawahjuesa, R.J. Gorte, D. De Olivera, L.Y. Lau, Catal. Lett. 82 (2002) 155–160.
- [38] N. Khandan, M. Kazemeini, M. Aghaziarati, Appl. Catal. A 349 (2008) 6–12.
- [39] Y. Fu, T. Hong, J. Chen, A. Auroux, J. Shen, Thermochim. Acta 434 (2005) 22.
- [40] G. Laugel, X. Nitsch, F. Ocampo, B. Louis, Appl. Catal. A: Gen. 402 (2011) 139–145.
- [41] R.A. Keogh, R. Srinivasan, B.H. Davis, J. Catal. 151 (1995) 292–299.
- [42] K.W. Jun, H.S. Lee, H.S. Roh, S.E. Park, Bull. Korean Chem. Soc. 23 (2002) 803–806.
- [43] Y.S. Hsu, Y.L. Wang, A.N. Ko, J. Chin. Chem. Soc. 56 (2009) 314–322.
- [44] R. Srinivasan, T. Watkins, C. Hubbard, B.H. Davis, Chem. Mater. 7 (1995) 725–730.
- [45] S. Sahebdelfar, M. Kazemeini, F. Khorasheh, A. Badakhshan, Chem. Eng. Sci. 57 (2002) 3611–3620.
- [46] A. Corma, Curr. Opin. Solid State Mater. Sci. 2 (1997) 63–75.
- [47] B. Subramanian, V. Arunajatesan, C.J. Lyon, Stud. Surf. Sci. Catal. 126 (1999) 63–77.
- [48] B. Li, R.D. Gonzalez, Appl. Catal. A 165 (1997) 291–300.
- [49] I. Ferino, M.F. Casula, A. Corrias, M.G. Cutrufello, R. Monaci, G. Paschina, Phys. Chem. Chem. Phys. 2 (2000) 1847–1854.
- [50] G.D. Yadav, J.J. Nair, Microporous Mesoporous Mater. 33 (1999) 1–48.